Pergamon

Int. J. Heat Mass Transfer. Vol. 38, No. 5, pp. 863–873, 1995

0017-9310/95 $9.50 + 0.00

0017-9310(94)00204-5

Validation of the quench factor technique in predicting hardness in heat treatable aluminum alloys

JOHN D. BERNARDIN and ISSAM MUDAWAR†

Boiling and Two-phase Flow Laboratory, School of Mechanical Engineering, Purdue University, West Lafayette, IN 47907, U.S.A.

(*Received* 4 *January* 1994 *and in final form* 29 *June* 1994)

Abstract—This paper explores the relationship between the heat transfer mechanisms and metallurgical transformations associated with spray quenching in the heat treating of aluminum alloys. A method known as the quench factor technique is presented as a means for predicting the hardness and strength of aluminum alloys following a procedure of solution heat treatment with spray quenching and artificial age-hardening. It is shown that the only input parameter for predicting hardness of a particular alloy is its temperature–time history during quenching. Temperature–time quench data measured both in small specimens and a relatively large L-shaped specimen are combined with metallurgical transformation data for aluminum alloy 2024-T6 to predict Rockwell B hardness. The predicted hardness compares well with the values measured for both types of specimens. These results both demonstrate the validity of the quench factor technique and emphasize the need for tools which would facilitate accurate prediction of the temperature–time history during spray quenching. Such tools could ultimately enable the aluminum industry to produce parts with both large and uniform hardness and strength by careful manipulation of the sprays.

1. INTRODUCTION

Processing of materials is currently undergoing rapid advances in the industrial community. Increased competitiveness, the demand for higher performance, and an age of environmental and cost consciousness have forced industry to develop more efficient and effective techniques to produce better materials with less waste. The spray quenching of extrusions, continuous castings, and solution heat treatable alloys is one such process which is in dire need for improvement and optimization. The purpose of optimizing spray quenching is to cool a part as quickly as possible in order to obtain desired material properties while, at the same time, preventing the occurrence of excessive temperature gradients which can induce warping and part failure.

Following solution heat treatment, which consists of preheating to a temperature above the solvus, alloy parts are commonly quenched either in a fluid bath or by a deluge of water sprays. In the case of spray quenching, current practice calls for configuring of the sprays in a pattern that appears to provide the cooling necessary to produce hardness and/or strength requirements while, at the same time, minimize warping. Accomplishing this task often requires several trials to achieve an acceptable cooling performance.

The purpose of this study is to examine the relationship between the temperature–time (cooling) history of a quenched aluminum alloy part and the precipitation kinetics of the alloy. Using the *quench factor technique*, this relationship will be formulated in order to *predict* distributions of hardness and strength across complex-shaped aluminum alloy parts following heat treatment, an objective which has never been systematically demonstrated before. This objective is accomplished in two stages. First, the quench factor technique is validated for small specimens for the cases of spray quenching and air cooling. The quench factor technique is then used to predict hardness distribution in a relatively large L-shaped specimen.

1.1. *Temperature–time history during quenching*

The quenching phase of a heat treatment process requires rapid cooling of the alloy part with the aid of an appropriate cooling fluid, the quenchant. Surface temperatures at the onset of quenching are typically very large, corresponding to the film boiling regime. As shown in Fig. 1, which is illustrated here for the reference case of bath quenching, an insulating vapor blanket greatly slows the rate of cooling in the film boiling regime. Heat is rejected from the surface by a combination of conduction across the vapor blanket and, to a lesser extent, by radiation. The surface experiences an increase in the rate of cooling in the transition boiling regime as liquid begins to break through the vapor blanket and contact the surface. Cooling rate increases further in the nucleate boiling regime as the entire surface becomes available for liquid contact and vigorous boiling. Eventually, the

† Author to whom correspondence should be addressed.

NOMENCLATURE

C_t	critical time for precipitation obtained from the C-curve	Greek symbols	
H	hardness	ζ	precipitation fraction
HR	hardness ratio, $(H-H_{min})/(H_{max}-H_{min})$	ζ_C	precipitation fraction corresponding to C-curve
k_i	empirical constants in equation (1)	σ	strength
R	universal gas constant	τ	quench factor.
T	temperature	Subscripts	
t	time.	max	maximum
		min	minimum.

cooling rate greatly diminishes in the single-phase regime as the surface temperature decreases asymptotically to the quenchant temperature. The temperature–time history (also called cooling curve or quench curve) illustrated in Fig. 1 is typical for points on or close to the surface since these points respond rapidly to the quench. However, points deeper in the part will have a delayed response and temperature–time histories which may differ greatly from points near the surface. Factors affecting the temperature–time history at a given point in the quenched part include location, thermal properties, and the part shape and thermal mass. The temperature–time history can be easily determined at every point in the part provided the quenchant boiling curve for the surface is known [1].

The temperature–time history determines the time available for microstructural transformation at each temperature and is, therefore, the vital link between the material and heat transfer aspects of quenching. One can use temperature–time curves to compare cooling rates at different locations, and begin to assess the effects of both surface cooling rate and internal temperature gradients on the final material properties.

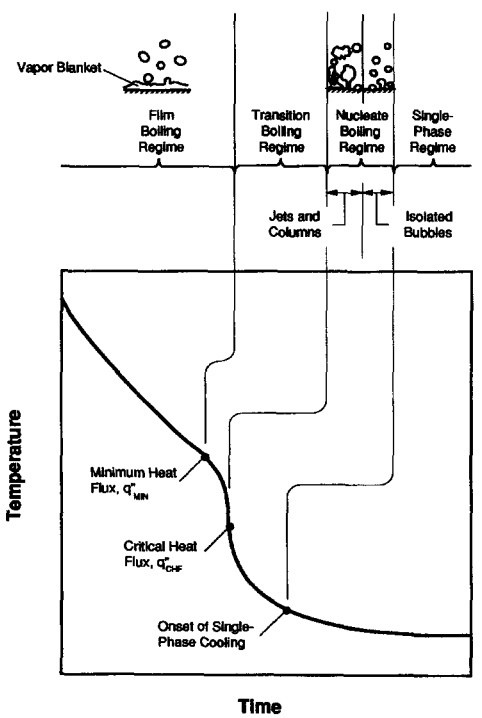

Fig. 1. Temperature–time history of a surface during quenching in a bath of liquid.

1.2. *Precipitation kinetics of heat treating*

It is through proper solid phase transformation that a wide range of material properties can be obtained from a given alloy for a broad range of applications. Various forms of heat treating are commonly used to achieve the proper phase transformation and, hence, desired material properties. In order to estimate the required cooling rate and assess the effectiveness of a quenching process during heat treating, an understanding of the metallurgical aspects of heat treating is required. These aspects can be described with the aid of the phase diagram, which indicates the various equilibrium phases that exist for a given temperature and component concentration, and temperature–time–transformation (TTT) diagram, which determines the percent completion of a given transformation (e.g. precipitation of hardening solutes) by accounting for the rate at which the transformation takes place. The TTT diagram uses phase transformation kinetics to describe how an alloy undergoes transition between two equilibrium states of the phase diagram.

Figure 2 shows a TTT diagram for a binary alloy of given concentration superimposed upon the phase diagram. The TTT diagram indicates the time required at each temperature for a given % of transformation to take place. The line between points a and b located in the plane of the phase diagram represents cooling of the alloy from a single-phase solid regime β to a two-phase solid regime $\alpha+\beta$. Shown in the temperature–time plane are curves corresponding to 100, 50 and 1% transformation to the two-phase mixture of α and β. The speed of phase transformation is dictated by the net effect of phase instability, diffusion and crystal growth [2]. While the rates of diffusion and crystal growth both decrease with decreasing tem-

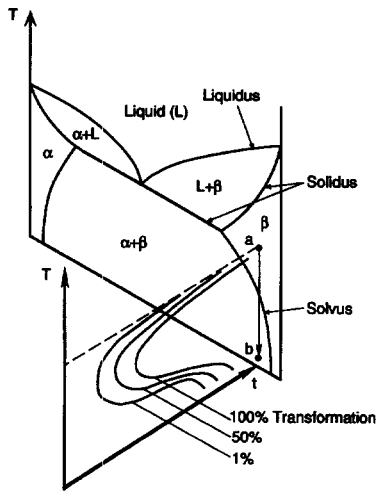

Fig. 2. Temperature–time–transformation (TTT) diagram for a binary alloy.

perature, the rate of phase instability increases at lower temperatures; hence the shape of the transformation curve, with a minimum (fastest rate) at some intermediate temperature. At high and low temperatures, precipitation rate is relatively low and a long period of time is required to transform a given amount of the material. At intermediate temperatures, precipitation rate is high; thus, a relatively short time is required to transform the same amount of the material.

Heat treating is a process aimed at altering metallurgical structure in order to achieve desired mechanical properties and/or reduce residual stresses. Increasing the hardness and strength of heat-treatable aluminum alloys is a three-step process: (1) solution heat treating, (2) quenching and (3) age-hardening. Solution heat treating involves heating the alloy to a temperature above the solvus but below the solidus, as illustrated in Fig. 2, which dissolves solid-phase hardening solutes such as copper and magnesium within the solid aluminum matrix. The desired end product of a heat treatment is an alloy that has a satisfactory homogeneity of hardening solutes throughout the part. This is dependent both upon cooling rate during quenching and the subsequent age-hardening.

Figure 3(a) shows temperature–time histories for an aluminum 2024 part corresponding to three different cooling processes: a slow air cooling, a fast water quench and an instantaneous (infinitely fast) quench. Slow air cooling allows ample time for precipitation to take place, facilitating massive precipitation of $CuAl_2$ (and $CuMgAl_2$) along aluminum grain boundaries. This pattern of precipitation is stable and cannot be altered with subsequent aging. The resulting alloy cannot, therefore, be hardened or strengthened with aging. Precipitates enhance hardness and strength of the alloy only when finely dispersed throughout the aluminum grains. Fine dispersion allows these precipitates to act as dislocation barriers which resist deformation of the part when subjected to stress. When they form on the grain boundaries due to slow cooling, these solutes cease to act as effective dislocation barriers, resulting in adverse effects on both hardness and strength.

Figure 3(a) shows the fast water quench providing little time for precipitation. Note that the few fine precipitate clusters that have formed are located within the grains and not along the grain boundaries. The resulting alloy is hardenable with subsequent aging. Only an infinitely fast quench, which is possible only with very thin specimens, would completely suppress precipitation, resulting in a supersaturated solid solution.

Following the quench, precipitation can be accelerated in a controlled manner by reheating the supersaturated solid solution to an intermediate temperature below the solvus and holding it at that temperature for a prescribed period of time. Figure 3(b) shows, when properly controlled, artificial age-hardening of a water quenched aluminum 2024 part following solution heat treating and quenching produces a large number of finely dispersed precipitates within the grains, resulting in a harder and stronger alloy. However, if the sample is held too long at the intermediate temperature, the precipitates will begin to coalesce, resulting in a weaker alloy. Overaging should, therefore, be avoided.

Thus, barring any appreciable stress concentration, the most desired quench is one that occurs at an infinitely fast rate, resulting in a supersaturated solid solution which can subsequently be manipulated into the desired fine dispersion of precipitates through proper age-hardening. Actual quenches typically fall short of producing a supersaturated solid solution. The amount of precipitation which occurs during the quench can be determined by contrasting the *time required* for precipitation, using the TTT diagram, with the *time available* for precipitation, using the temperature–time cooling history of the quenched part. Discussed later in this paper is how the quench factor technique can be used for estimating the extent of precipitation produced during an actual quench and the impact of this precipitation on hardness.

1.3. *C-Curve*

During the past eight years, a large scale intelligent materials processing test bed (described in the next section) was established at the Purdue University Boiling and Two-Phase Flow Laboratory to develop CAD-based process models that would enable the fabrication of aluminum alloy parts with maximum hardness and strength and minimum warping [3, 4]. The test bed encompasses several cross-disciplinary studies including spray quenching, non-contact temperature sensing, residual stress measurement and precipitation kinetics.

A primary tool which was employed in the test bed CAD system is a particular form of the TTT diagram

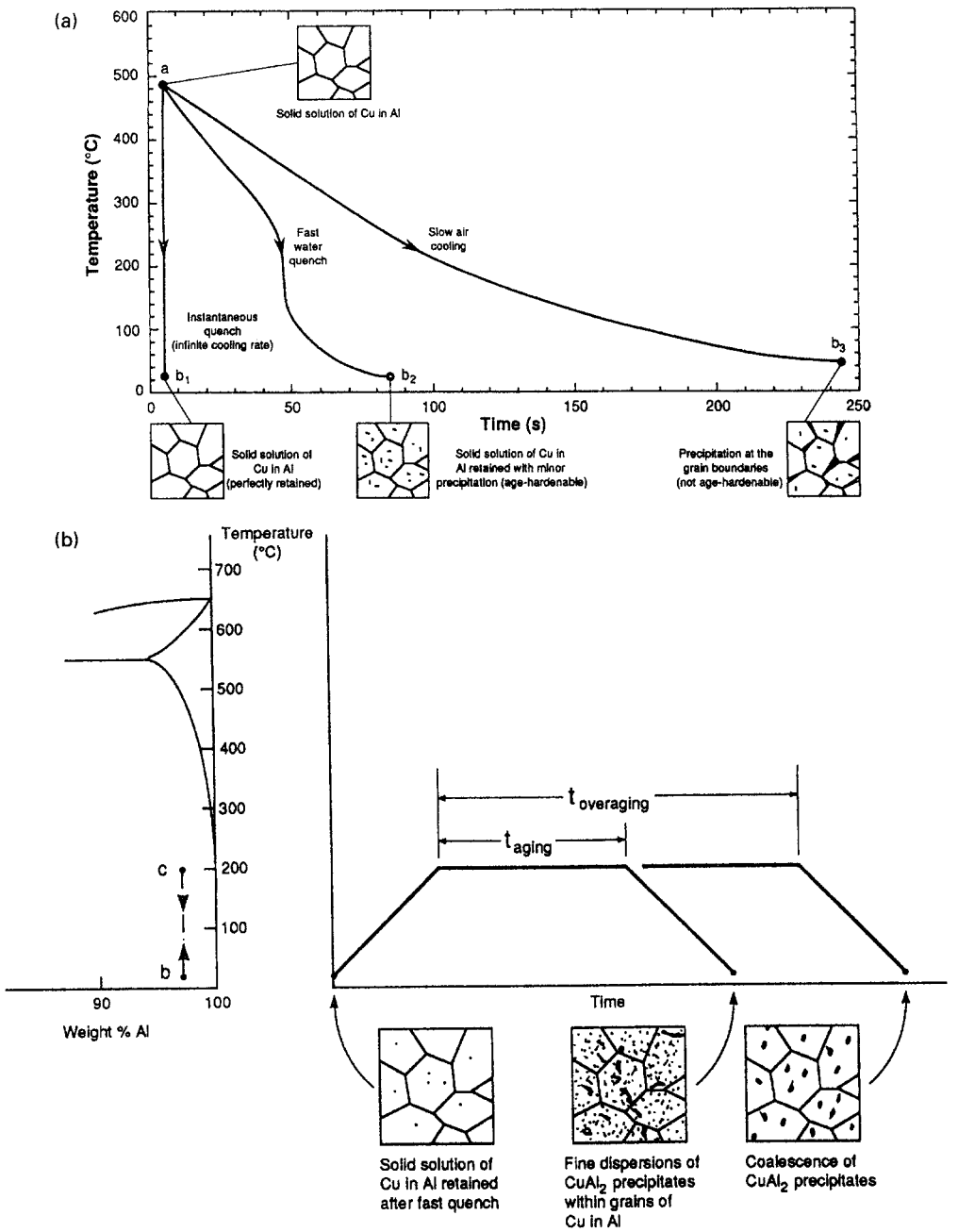

Fig. 3. (a) Precipitation of hardening solutes produced by various cooling techniques. (b) Proper aging and overaging of an aluminum–copper alloy following a fast water quench (adapted from Shackelford [2]).

called the *C-curve*. The C-curve for aluminum 2024 was determined from a procedure called the *delayed quenching technique* (see refs. [5–7]). As illustrated in Fig. 4(a), to construct a C-curve, thin samples of the alloy are solution heat treated and quenched very rapidly in a salt bath to a given temperature, held at that temperature for a period of time, and rapidly quenched again, this time to room temperature. The sample is then age-hardened and its hardness measured. This procedure is repeated for a large number of samples at different holding temperatures and holding times. Figure 4(b) shows three different C-curves, each corresponding to a different hardness ratio, *HR*. As shown in Fig. 4(b), the C-curve is named as such because it is a C-shaped locus of points on temperature–time coordinates corresponding to equal hardness values. The general features of the TTT diagram are clearly manifested in the C-curve: high and low temperatures require large times to attain a given precipitation, ζ_C, that would result in the desired hard-

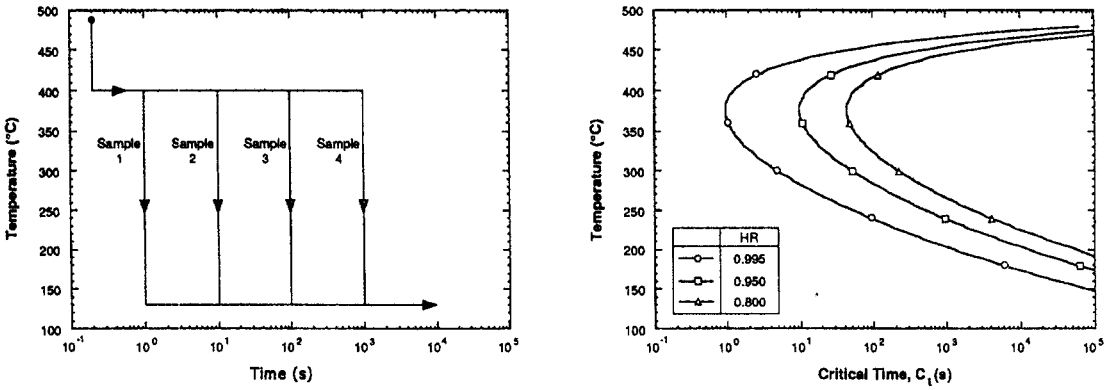

Fig. 4. (a) Delayed quenching technique used to determine the C-curve and (b) C-curves for aluminum 2024-T6.

ness, while intermediate temperatures demand much smaller times for the same precipitation and same hardness.

The general form of the C-curve is [8]

$$C_t = -k_1 k_2 \exp\left(\frac{k_3 k_4^2}{RT(k_4 - T)^2}\right)\exp\left(\frac{k_5}{RT}\right) \quad (1)$$

where C_t is the critical time required to achieve a given amount of precipitation or given hardness, R is the universal gas constant (8.314 J gmol^{-1} K^{-1}), T is the absolute temperature in Kelvins, k_1 is the natural logarithm of the unprecipitated fraction, $1-\zeta_C$, or hardness ratio, HR, *corresponding to the particular C-curve* and k_2, k_3, k_4 and k_5 are constants related to reciprocal of the number of nucleation sites, energy required to form a nucleus, solvus temperature, and activation energy for diffusion, respectively. While C-curves for different aluminum alloys are similar in shape, their relative positions on temperature–time coordinates depend on the values of k_2–k_5 which are determined experimentally for each alloy. For 2024-T6, k_1 corresponding to an unprecipitated fraction, $1-\zeta_C$, or hardness ratio, HR, of 0.995 is -0.00501, $k_2 = 2.38 \times 10^{-12}$ s, $k_3 = 1.31 \times 10^3$ J gmol^{-1}, $k_4 = 8.40 \times 10^2$ K, $k_5 = 1.47 \times 10^5$ J gmol^{-1} [6].

2. QUENCH FACTOR TECHNIQUE

When an aluminum alloy is quenched following solution heat treatment, mechanical properties develop which are strongly dependent upon the rate of cooling. As indicated earlier, the rate at which the alloy is quenched dictates the time available for precipitation of the hardening solutes. Isothermal precipitation kinetics [9] indicate that, at a given temperature during a quench, the fraction of precipitation, ζ_t, is dependent upon the ratio of actual time, t, dictated by the rate of cooling, to the critical time for precipitation, C_t determined from the C-curve:

$$\zeta_t = 1 - \exp\left(\frac{k_1 t}{C_t}\right). \quad (2)$$

Because k_1 is a negative number, a slow quench would increase t, resulting in greater precipitation and reduced hardness. Since an actual quench involves large temperature changes, the overall phase transformation following the quench is the sum of all differential transformations determined using equation (2).

As shown in Fig. 5, the quench factor technique approximates an actual quench (measured experimentally in the present study) as a series of isothermal quenches, thus allowing transient transformations to be predicted from the isothermal precipitation kinetics described by equation (2). Over a period Δt_i, equation (2) gives the change in the fraction of precipitation as

$$\ln(1-\zeta_{t_i+\Delta t_i}) - \ln(1-\zeta_{t_i}) = \frac{k_1}{C_{t,i}}\Delta t_i. \quad (3)$$

Writing equation (3) for every time increment during the quench and adding the resulting equations for all the increments yields an expression for the cumulative precipitation, ζ, at the end of the quench:

$$\ln(1-\zeta) = k_1\left(\frac{\Delta t_1}{C_{t,1}} + \frac{\Delta t_2}{C_{t,2}} + \frac{\Delta t_3}{C_{t,3}} + \cdots\right)$$

$$= k_1 \sum \frac{\Delta t_i}{C_{t,i}}. \quad (4)$$

Figure 5 shows, for aluminum 2024, the incremental precipitation corresponding to the infinitesimal isothermal step quenches in the temperature–time (cooling) curve. Also shown is how these precipitation increments can be added to give a total amount of precipitation for that particular temperature–time curve.

The quench factor itself is a dimensionless parameter defined as the sum of all the right-hand-side terms of equation (4) [8, 10]:

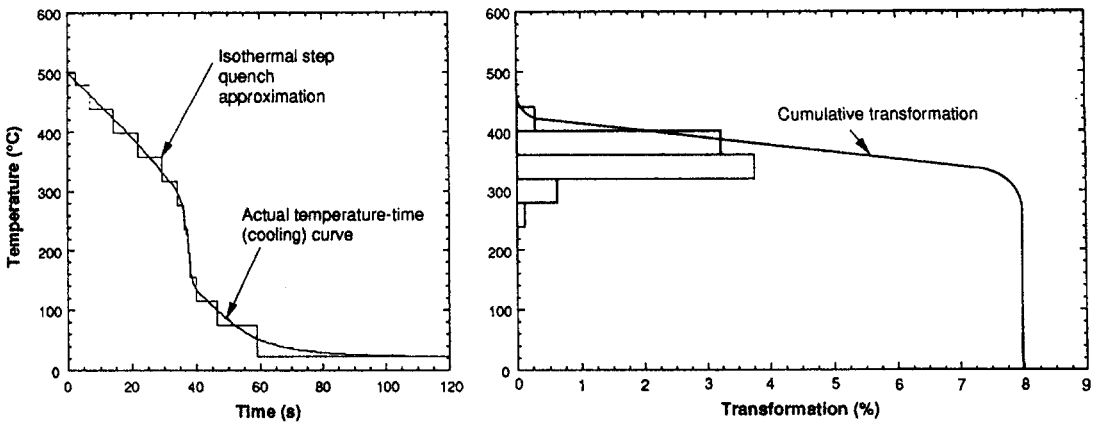

Fig. 5. Continuous cooling curve approximated as a series of isothermal quenches and % of phase transformation and cumulative transformation at temperatures corresponding to the isothermal step quenches.

$$\tau = \frac{\ln(1-\zeta)}{k_1} = \int_{t_0}^{t_f} \frac{dt}{C_t} \approx \sum \frac{\Delta t_i}{C_{t,i}}. \quad (5)$$

Recall that the C-curve is developed from the delayed (not actual) quenching technique using very small samples of the alloy. Each point on the C-curve for a given hardness ratio corresponds to a constant precipitation fraction, ζ_C. Equation (5) indicates $\tau = 1$ if ζ at the end of an actual quench is equal to ζ_C. k_1, as indicated earlier, is the natural logarithm of the unprecipitated fraction, $1-\zeta_C$, corresponding to the C-curve itself. With an actual quench, $\zeta > \zeta_C$; τ for an actual quench is, therefore, greater than unity.

The integral in equation (5) can be discretized by dividing the cooling curve into a series of small time increments. Next, average temperatures corresponding to each of the time increments are used to determine the corresponding critical times from the C-curve.

It should be noted that, while only the quench history is required in calculating the quench factor, the effects of solution heat treatment and artificial aging are implicit in the C-curve itself.

Since the strength of precipitation-hardenable aluminum alloys is proportional to hardness [11] and because hardness is dependent upon the unprecipitated fraction of hardening solutes, simple relationships can be obtained for both strength [8] and hardness [6] using equations (4) and (5):

$$\frac{\sigma-\sigma_{min}}{\sigma_{max}-\sigma_{min}} = \frac{H-H_{min}}{H_{max}-H_{min}} = 1-\zeta = \exp(k_1\tau) \quad (6)$$

where σ_{max} and H_{max} are, respectively, the maximum values of strength and hardness which are obtained by solution heat treating a thin specimen of the alloy followed by an instantaneous quench to room temperature and a subsequent age-hardening, and σ_{min} and H_{min} are, respectively, the strength and hardness obtained by very slow controlled cooling. For aluminum 2024, $H_{max} = 78.4$ (Rockwell B hardness) and $H_{min} = 2.2$ [6]. Equations (5) and (6) indicate, since k_1 is negative, a very fast quench greatly decreases τ, increasing both strength and hardness. The present study utilizes hardness measurements instead of strength measurements to validate the quench factor technique due to the relative ease of obtaining hardness measurements in complex-shaped specimens and because hardness ratio is equal to strength ratio for age-hardenable aluminum alloys [11].

The relative temperature regions of the temperature–time cooling curve and the corresponding regions of the C-curve are of paramount importance to any quenching process. When both curves are available, one can intuitively judge in which temperature range the precipitation rate is high and, therefore, where a fast cooling rate is required if a heat treatable alloy is to attain large hardness and large strength. Quench (cooling) rate has no effect on the material properties in temperature regions of the C-curve where precipitation rate is low, i.e. in regions of low and high temperature. During a quench, an aluminum alloy experiences drastically different cooling rates as it progresses through the different boiling regimes, Fig. 1, which is evident in slope changes of the temperature–time cooling curve. In order to increase both hardness and strength, it is desired to manipulate the temperature–time cooling history (by modifying the external spray conditions) in order to achieve the fastest cooling rate at the nose of the C-curve associated with the fastest precipitation rate.

This can be represented mathematically by expressing the quench factor, equation (5), as

$$\tau = \int_{t_0}^{t_f} \frac{dt}{C_t} = \int_{T_0}^{T_f} \frac{1}{C_t(T)\left(\frac{dT}{dt}\right)} dT. \quad (7)$$

Equation (7) suggests the quench factor can be minimized by maximizing the product of cooling rate and corresponding critical time from the C-curve. Thus,

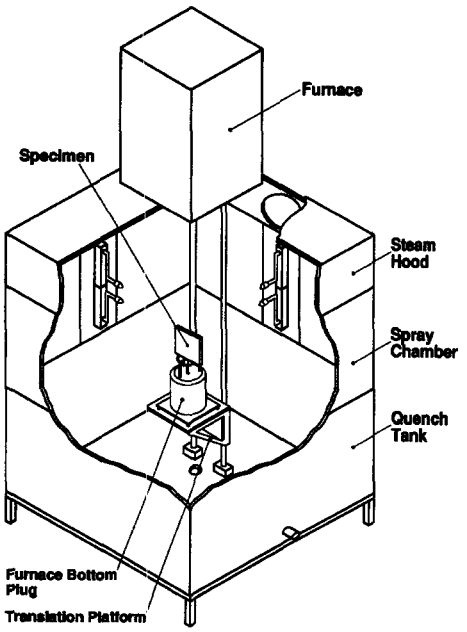

Fig. 6. Cut-away view of the materials processing test bed.

in a temperature region where the critical time, $C_t(T)$, is small, dT/dt must be made as large as possible. This simply implies *better hardness and strength can be developed by modifying the spray system such that the fastest cooling regimes, transition boiling and nucleate boiling, coincide, as much as possible, with the nose of the C-curve.*

By matching the nose of the C-curve with the quickest part of the quench curve, small errors will be amplified when determining the quench factor using equation (5). Thus, fine discretization must be employed when approximating the quickest cooling region. This is generally not a problem since modern data acquisition systems can record temperature data with millisecond resolution.

In addition to optimizing the quenching process in order to obtain a harder and stronger alloy, knowledge of the critical nose region of the C-curve can facilitate additional control of the spray system *during the quench* to reduce thermal stresses. For example, after exiting the critical temperature region, since the hardness will not change significantly by the quench, the quench rate could be slowed (by reducing the spray flow rate) in order to reduce temperature gradients within a thick part.

3. EXPERIMENTAL METHODS

3.1. *Materials processing test bed*

The aluminum test specimens were heat-treated in a large scale materials processing test bed which features a high temperature furnace and spray quenching chamber, both supported upon a $1.35 \times 1.35 \times 2.69$ m high steel frame, Fig. 6, an external water delivery system, and a console housing a CAD workstation, data acquisition system, video monitors and control panels. A high temperature Lindberg 54857-V tube furnace equipped with a three-zone programmable controller was used both for solution heat treating and age-hardening. The specimen was mounted onto a translation platform and raised with the aid of a counterweight pulley system into the furnace for heating, then lowered into the spray chamber for quenching, raised again into the furnace for age-hardening, and lowered a second time into the spray chamber where it was quenched to room temperature, all in accordance with the desired heat treating schedule.

The spray chamber was constructed of optical grade Lexan sheet which facilitated video monitoring of the test specimen during the quench. Four nozzle racks, each containing a vertical array of three flat fan spray nozzles, provided the desired spray pattern which could be individually controlled based upon the shape and size of specimen. Water from an aluminum tank situated directly below the quench chamber was routed to the spray nozzles by a Gould centrifugal pump rated to deliver up to 25.2×10^{-3} m^3 s^{-1} (40 gpm) of water at 689 kPa (100 psi).

To test the validity of the quench factor technique in predicting hardness, two types of specimens were fabricated from extruded aluminum 2024, thin squares and a relatively large L-shaped specimen.

3.2. *Square specimens*

The first type of test specimen consisted of 4.76 mm thick squares measuring 76.20 mm on the side, which were mounted onto the translation platform with the aid of a small screw as shown in Fig. 7(a). Each square was instrumented with a chromel–alumel (type K) thermocouple set in magnesium oxide insulation inside a 0.81 mm Inconel sheath. The exposed thermocouple bead was pressed into a 1.02 mm diameter hole which was prepacked with high thermal conductivity boron nitride powder to ensure good thermal contact between the bead and specimen.

The square specimens were subjected to a full heat treatment schedule as recommended by the American Society of Metals [11] and Kim [6] for a T6 temper. Quenching was accomplished by flat fan sprays which impacted one side of the specimen. The spray nozzles were located 32.4 cm from the sample surface and operated at 552 kPa (80 psi), producing drops with a Sauter mean diameter of 0.137 mm which impacted the surface with a mean velocity of 20.6 m s^{-1}. One of the square samples was cooled in open air following the solution heat treating in order to test the validity of the quench factor technique in predicting the effects of massive precipitation resulting from poor cooling.

3.3. *L-Shaped specimen*

The second type of test specimen was a relatively large extrusion which was machined into the L-shaped cross-section shown in Fig. 7(b) and carefully polished prior to heat treating. The relatively large thermal mass ratio of the thick section relative to the thin

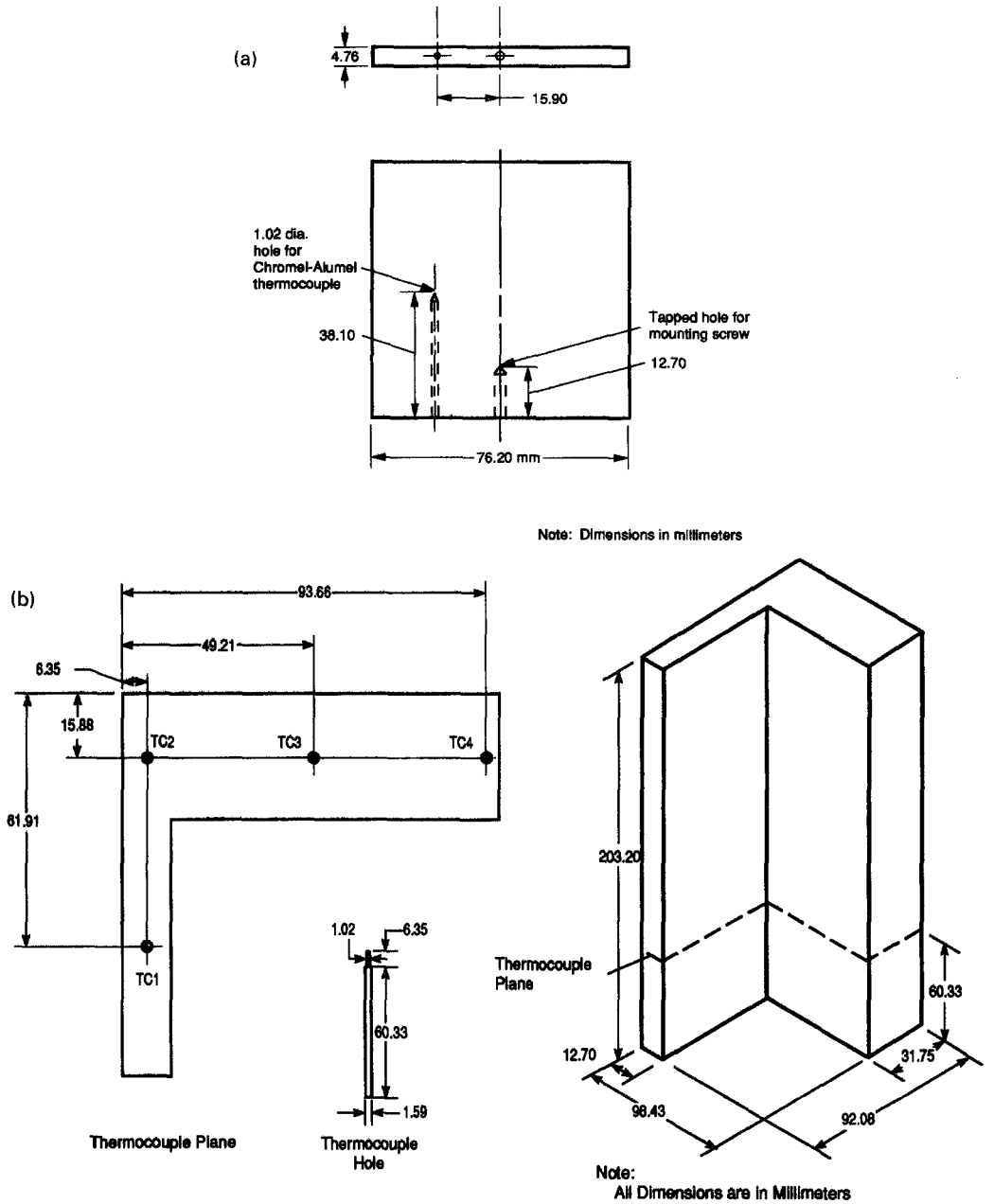

Fig. 7. Construction of (a) square specimens and (b) L-shaped test specimen.

section enabled the study of the effects of cooling rate and cooling uniformity on the hardness distribution. Four thermocouples were embedded in the same horizontal plane 60.33 mm from the lower edge of the specimen as detailed in Fig. 7(b). These thermocouples were identical in construction and installation to those used in the square specimens.

The L-shaped specimen was quenched along the outer surface of the thin section only in order to induce some nonuniformity both in cooling rate and the resulting hardness following the age-hardening. The thin section was quenched by a vertical array of three flat fan sprays formed by nozzles positioned 30.5 cm from the surface. Each spray was operated at 552 kPa (80 psi), producing drops with a mean velocity of 13.5 m s^{-1} and a Sauter mean diameter of 0.286 mm. Some overlap between the impact areas of adjacent sprays was carefully optimized to ensure a two-dimensional volumetric spray flux distribution along the sprayed surface; details of this optimization can be found elsewhere [12].

The L-shaped specimen was heat treated in accordance with recommendations of the American Society of Metals [11]. The specimen was solution heat treated at a uniform temperature of 495°C for a period of 160 min, quenched to room temperature and held at that

temperature for 2 h, age-hardened at 190°C for 16 h, and spray quenched again to room temperature.

Upon completion of the age-hardening, the L-shaped specimen was cut open using a wet band saw along a plane near that of the thermocouples. The sawed surface was then lightly milled, sanded, and hand polished to produce a smooth surface for the hardness measurements. During the cutting and milling, abundant amounts of coolant and lubricating oil were used to preclude any appreciable rise in surface temperature. Three grades of sandpaper of decreasing roughness, 360 grit, 600 grit and crocus cloth, were used to remove the relatively large surface roughness features. Finally, a Simichrome compound was used to produce a mirror-polished finish for the hardness measurements. To verify that the sawing and milling did not alter the hardness of the material, hardness measurements were also made, prior to sawing the specimen, along the outer surfaces at locations near the internal hardness measurement locations.

An Oko-Seiki model 3R hardness tester was used to measure the Rockwell B hardness of the specimens. A reference specimen with a Rockwell B hardness of 83.6 was used to calibrate the hardness tester prior to performing measurements on the test specimens. Four hardness measurements made in the vicinity of each reference measurement location of the L-shaped sample were averaged and compared to the hardness predictions made using the quench factor technique and the temperature–time history measured by the thermocouples during the quench.

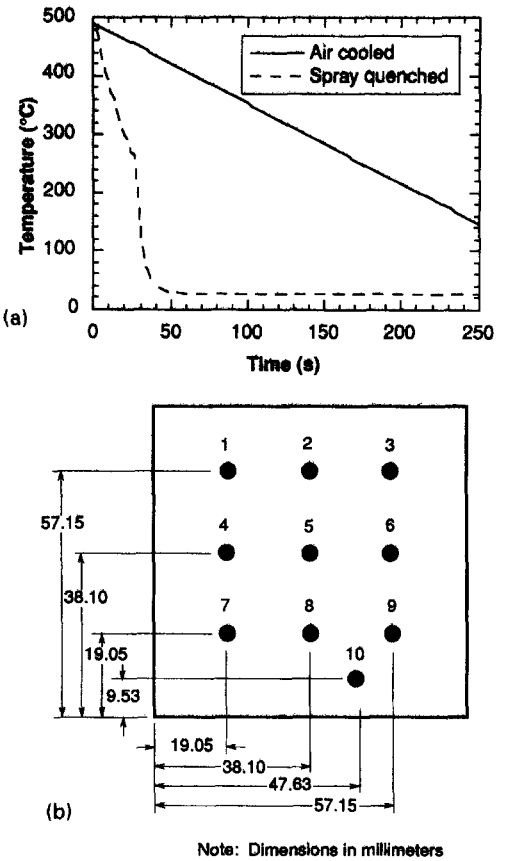

Fig. 8. (a) Measured temperature–time histories and (b) hardness measurement locations for the square specimens.

4. RESULTS AND DISCUSSION

The measured hardness results are presented to validate the quench factor technique which was used to predict hardness utilizing the measured temperature–time cooling curve. All hardness values presented in this section correspond to the Rockwell B scale.

4.1. *Validation of quench factor technique—small square specimen results*

As indicated earlier, two square specimens were tested. The heat treatment for the two samples differed only in that one sample was air cooled while the other was spray quenched following the solution heat treatment. The measured temperature–time histories in Fig. 8(a) indicate vast differences in cooling rate between the two specimens. Figure 8(b) shows locations for the hardness measurements for both cases. The corresponding hardness results are given in Table 1 which shows, as to be expected, a nearly uniform hardness across the surface of each specimen because of the small thermal mass of the specimens used. The average Rockwell B hardness of 78.2 for the spray quenched specimen is considerably higher than the value of 54.25 for the air cooled specimen, clearly indicating the importance of fast cooling in enhancing hardness. The hardness for the spray quenched specimen fits well within the range of 74.5–83.5 given in the ASM Handbook [11] for acceptable hardness values for aluminum 2024 with a T6 temper, and is nearly identical to the value obtained by Kim [6], 78.4, for instantaneous quenching of very thin Al-2024-T6 specimens.

Table 2 compares the hardness values measured at location 4 (surface location closest to the thermocouple) to the value predicted using the quench factor technique based upon the temperature–time

Table 1. Rockwell B hardness measurements for the air cooled and spray quenched Al-2024 square specimens

Measurement location	Air cooled Rockwell B hardness	Spray quenched Rockwell B hardness
1	54.0	78.5
2	53.5	79.5
3	52.5	79.5
4	55.5	78.0
5	54.0	78.5
6	54.5	79.0
7	54.5	77.5
8	55.0	78.5
9	55.0	77.5
10	54.0	75.5
Average	54.25	78.2

Table 2. Measured Rockwell B hardness results for the Al-2024 square specimens compared to predictions based upon the measured temperature–time history

	Measured at location 4	Predicted for location 4
Air cooled Rockwell B hardness	55.5	55.4
Spray quenched Rockwell B hardness	78.0	74.4

history measured by the thermocouple. For both the air cooled and spray quenched specimens, deviation of the predicted hardness from the measured value is within 5%, which demonstrates the validity as well as accuracy of the quench factor technique.

4.2. *Predictions of quench factor technique for the L-shaped specimen*

Temperature–time histories corresponding to the four thermocouples in the L-shaped specimen are shown in Fig. 9(a). As expected, the thin section cooled the quickest, as indicated by the temperature–time data corresponding to thermocouple TC1. Conduction to the thin section caused TC2 to cool much faster than the other thermocouples in the thick section, TC3 and TC4, which maintained fairly equal cooling rates.

Figure 9(b) displays averages of the surface and internal hardness measurements made along the thermocouple plane of the L-shaped specimen. Measurements were not possible for the backside of the thin section of the specimen because of clearance limitations imposed by the hardness tester. The hardness averages reveal a trend of relatively larger hardness in the thin section and smaller hardness in the thick section, since the spray impacted only the outer surface of the thin section. A slight increase in hardness along the right surface of the thick section can be attributed to an observed slight recirculation of mist from the sprayed surface to the right side of the thick section, which was caused by confinement of the spray in the quench chamber.

Nonuniform cooling rate throughout the ther-

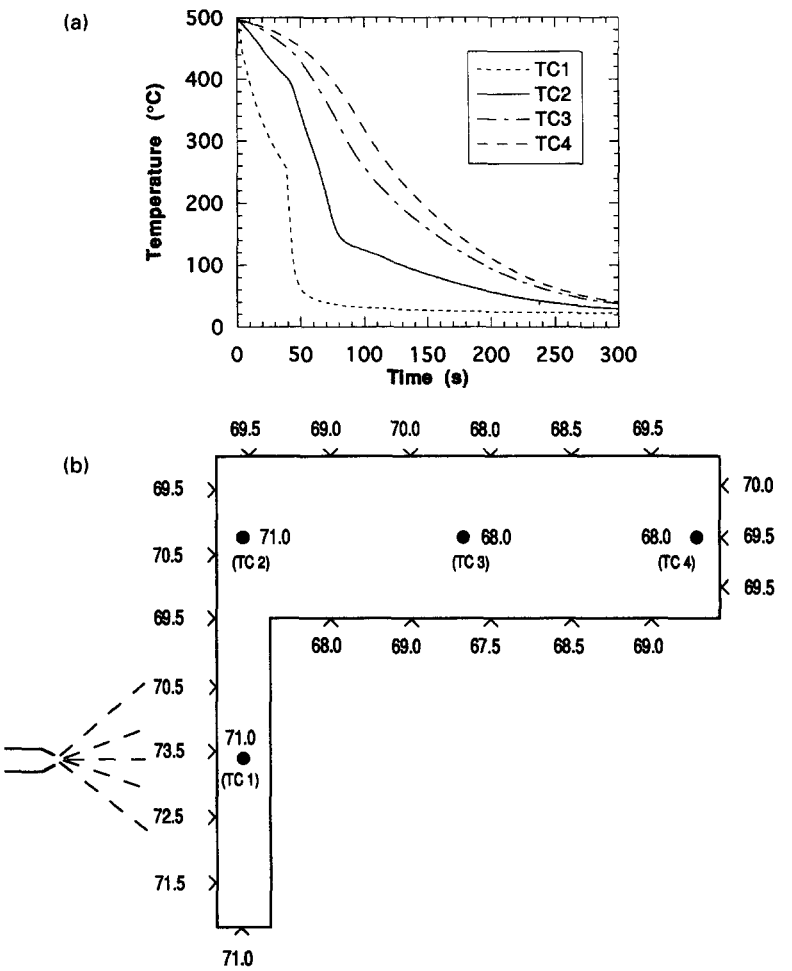

Fig. 9. (a) Measured temperature–time history for thermocouple locations within the L-shaped specimen and (b) external and internal Rockwell B hardness measurement averages along the thermocouple plane of the L-shaped specimen.

Table 3. Measured Rockwell B hardness results for the Al-2024-T6 L-shaped specimen compared to predictions based upon the measured temperature–time history

Thermocouple location	Measured Rockwell B hardness	Predicted Rockwell B hardness
TC1	71.0	72.9
TC2	71.0	70.7
TC3	68.0	68.4
TC4	68.0	66.8

mocouple plane is also reflected by the nonuniform hardness predictions as shown in Table 3. Of the four thermocouple locations, the highest hardness, 72.9, was predicted for TC1, which corresponds to the fastest cooling rate, while the lowest hardness, 66.8, was predicted for the slowest cooling thermocouple location, TC4. Table 3 shows excellent agreement between the predicted and measured values corresponding to each of the four thermocouple locations. The predictions are all within 3% of the measurements; some of these differences can be attributed to the 1.2% error associated with the calibration of the hardness tester as well as the error associated with measuring the C-curve itself.

The results of the L-shaped specimen demonstrate not only the validity of the quench factor technique in predicting hardness, but also its effectiveness as a means for optimizing quenching of complex-shaped aluminum parts in the production of alloys with both superior hardness and strength and predictable performance.

5. CONCLUSIONS

This study explored the relationship between the temperature–time history of aluminum parts and metallurgical transformations associated with spray quenching. Key conclusions from the study are as follows.

(1) Achieving superior hardness and strength in aluminum alloys demands very rapid quenching following the solution heat treatment. The quench rate must be high enough to retard precipitation of the alloying elements so that controlled precipitation may occur during aging. Since precipitation rate is fastest in the temperature region corresponding to the nose of the C-curve, quenching rate must be maximized in the same region by having the fastest cooling regimes of the quench, transition boiling and nucleate boiling, coincide, as much as possible, with the nose region of the C-curve through careful manipulation of the spray system.

(2) Observations concerning precipitation and cooling behavior through the C-curve and quench curve indicate it is possible to greatly reduce the temperature gradients responsible for stress concentration within an aluminum part during quenching, without compromising hardness or strength, by reducing the spray flow rate as the part temperature drops below the nose region of the C-curve.

(3) For alloys with known C-curves, the quench factor technique enables accurate determination of hardness (and strength) so long as their temperature–time history during the quench is known. Thus, developing tools for accurate prediction of quench history is of paramount importance to improving mechanical properties of alloy.

(4) The quench factor technique is a viable means for predicting hardness distribution in complex-shaped aluminum parts following heat treatment. The technique enables the assessment of effectiveness of an existing quenching process, and may lend itself to optimizing the quenching process in pursuit of both superior and uniform properties.

Acknowledgements—Financial support for this work by the National Science Foundation and Purdue University Engineering Research Center for Intelligent Manufacturing Systems is gratefully appreciated. The authors also thank Messrs Jerry Hagers and Rudolf Schick of Spraying Systems Company and Gerry Dail of ALCOA for their technical assistance.

REFERENCES

1. I. Mudawar and T. A. Deiters, A universal approach to predicting temperature response of metallic parts to spray quenching, *Int. J. Heat Mass Transfer* **37**, 347–362 (1994).
2. J. F. Shackelford, *Introduction to Materials Science for Engineers* (3rd Edn). Macmillan, New York (1992).
3. T. A. Deiters and I. Mudawar, Optimization of spray quenching for aluminum extrusion, forging or continuous casting, *ASME J. Heat Treating* **7**, 9–18 (1989).
4. W. P. Klinzing, J. C. Rozzi and I. Mudawar, Film and transition boiling correlations for quenching of hot surfaces with water sprays, *ASME J. Heat Treating* **9**, 91–103 (1992).
5. W. L. Fink and L. A. Willey, Quenching of 75S aluminum alloy, *Trans. Am. Inst. Mining Metall. Engrs* **175**, 414–427 (1947).
6. J. S. Kim, Prediction of the influence of water spray quenching on the age-hardenability of aluminum alloy 2024, Masters Thesis, School of Materials Science and Engineering, Purdue University, West Lafayette, IN (1989).
7. J. D. Bernardin, Intelligent heat treatment of aluminum alloys: material, surface roughness, and droplet–surface interaction characteristics, Masters Thesis, School of Mechanical Engineering, Purdue University, West Lafayette, IN (1993).
8. J. W. Evancho and J. T. Staley, Kinetics of precipitation in aluminum alloys during continuous cooling, *Metall. Trans.* **5**, 43–37 (1974).
9. M. Avrami, Transformation–time relations for random distribution of nuclei, *J. Chem. Phys.* **8**, 212–224 (1940).
10. J. W. Cahn, Transformation kinetics during continuous cooling, *Acta Metall.* **4**, 572–575 (1956).
11. American Society of Metals, Heat treating, in *ASM Handbook* (10th Edn), Vol. 3. ASM International, Materials Park, OH (1991).
12. D. D. Hall, A method of predicting and optimizing the thermal history and resulting mechanical properties of aluminum alloy parts subjected to spray quenching, Masters Thesis, School of Mechanical Engineering, Purdue University, West Lafayette, IN (1993).